Earth, Planets and Space

FULL PAPER Open Access

Estimating frequency-dependent shear wave velocity in near-surface sediment based on seismic interferometry

Hao Zhang[1], Yang Shi[1], Hongjun He[1], Hanwen Ji[1] and Yu Miao[1,2*]

Abstract

Near-surface seismic shear wave is a basic tool for seismic investigations. However, its frequency-dependent property is not fully investigated, especially by the in situ observation method. Here, we develop the seismic interferometry with a moving frequency window to process the natural seismic signals recorded by the KiK-net network. It is observed that the phase velocity of the shear wave decreases sharply as the frequency increases in the low-frequency range, and remains constant in the high-frequency range. The observed dispersion phenomenon presents a challenge to existing site effect prediction theories, while also providing an observational reference for understanding how the shear wave propagates in near-surface sediment.

Key points

- Moving-frequency-window seismic interferometry is developed to extract the frequency-varying information of the ground motion.
- It is firstly observed that the shear wave velocity in near-surface sediment is strongly frequency-dependent.
- The phase velocity of the shear wave decreases sharply in the low-frequency range as the frequency increases.

Keywords Seismic shear wave, Seismic interferometry, KiK-net, Dispersion, Near-surface sediment

*Correspondence:
Yu Miao
miaoyu@hust.edu.cn
Full list of author information is available at the end of the article

Graphical Abstract

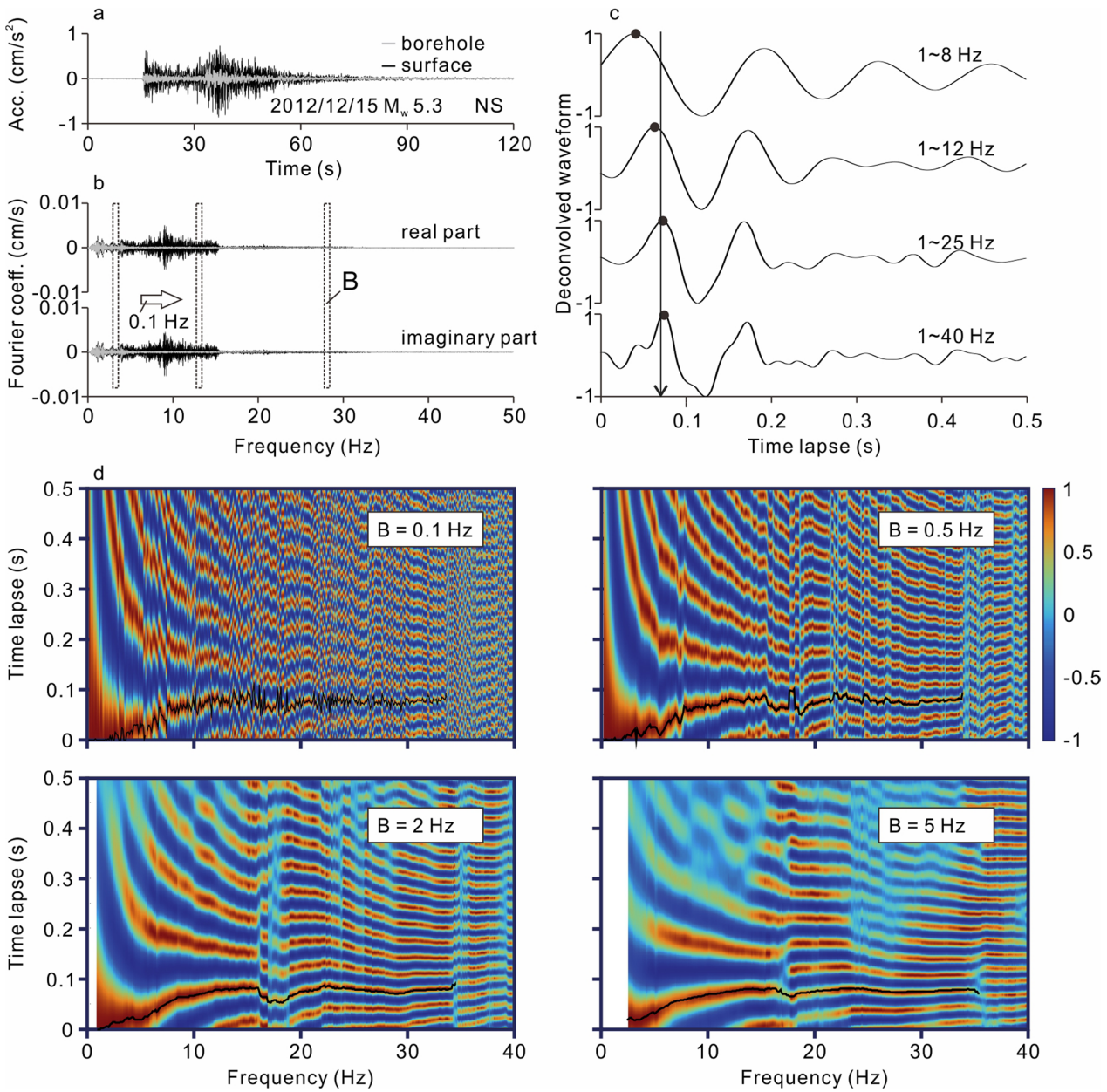

Introduction

Near-surface seismic shear wave is widely used in the in the study of site effect, seismic hazard analysis, seismic engineering design, seismic exploration, and seismic tomography (Bonilla et al. 2019; Peng and Ben-Zion 2006; Field et al. 1997; Rydelek and Tuttle 2004; Wang et al. 2021; Kim and Lekic 2019; Kaklamanos and Bradley 2018; Chabyshova and Goloshubin 2014). Clarifying the frequency-dependent properties of near-surface seismic shear wave is the basis for the higher precision seismic investigations. Theoretical and the experimental researches on this aspect have been ongoing for decades (Aki and Richards 1980; Ba et al. 2016; Borgomano et al. 2017; Müller et al. 2010), but the research based on the in situ observations are sparse, because it is generally believed that the natural ground motion has strong instability and randomness, making it difficult to separate different frequency components for analysis

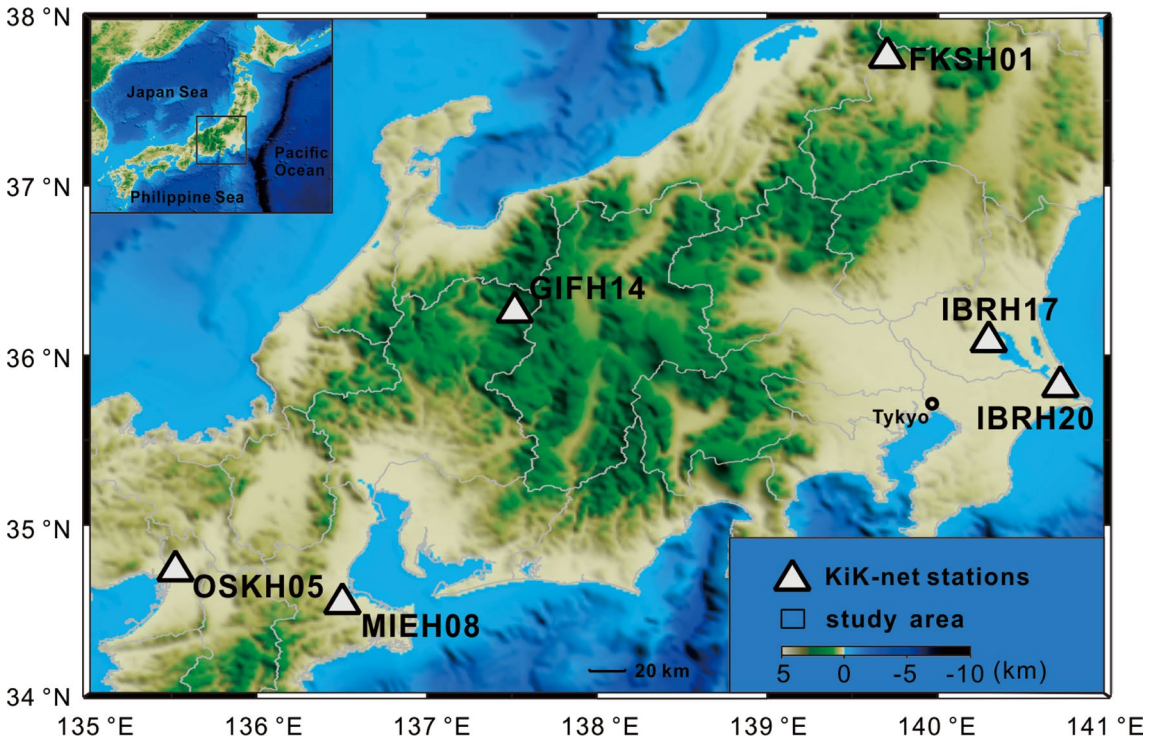

Fig. 1 Topographic map of Japan and KiK-net stations used in this study. Each station consists of a borehole and a pair of seismic sensors deployed at the bottom and surface

(Kaklamanos and Bradley 2018; Zhu et al. 2022; Thompson et al. 2012).

By applying the resonant oscillation, sonic test, and ultrasonic test to the geomaterial samples in a large frequency range (0.01 Hz to 1 MHz), it is obtained that variation of the compression-wave velocity is about 5–30%, and the shear wave velocity generally experiences less than 5% change (Ba et al. 2016; Borgomano et al. 2017; Müller et al. 2010). The experimental results are in accordance with the material-dispersion theory, which refers to that the frequency-varying velocity is caused by the frequency-varying attenuation of the geomaterial (Müller et al. 2010; Carcione 2007). In the material-dispersion theory, the ideal geomaterial is composed by two parts: the elastic homogeneous rock frame and the pore viscous fluid, corresponding to the spring and pot of the ideal soil model (Müller et al. 2010; Carcione 2007). The viscous properties of porous materials are frequency-dependent which makes the velocity vary with frequency.

Using the in situ vibrator seismic profile test, Sun et al (2009) reported the shear wave velocity increases by about 6% in the 8–180 Hz frequency band, and Koedel and Karl (2020) reported that the shear wave velocity increases by about 5% in the 25–80 Hz frequency band. They explained the obtained velocity change with the material dispersion theory, and calculated the site damping value based on the relationship between the damping and velocity in the material dispersion theory.

However, although the experiments and theory match well, and have received support from the in situ tests, there are still several issues that need to be considered. (1) The laboratory material sample is perturbed and the in situ condition is lost, which result in the difficulty in depicting the structural characteristics of the sediment, particularly the inhomogeneity caused by the ground stress and modulus distribution. (2) Limited by the energy of the in situ artificial source, the information in the low-frequency range is missing, and most of the energy of the shear wave concentrates on the range (1–10 Hz). Therefore, it is necessary to investigate the frequency-dependent property of the near-surface seismic shear wave based on in situ observation method.

In this study, we aim to estimate the frequency-dependent velocity of near-surface seismic shear wave by performing the seismic interferometry to the natural seismic signals recorded at 6 sites in Japan. Firstly, we introduced the seismic data collected and provided

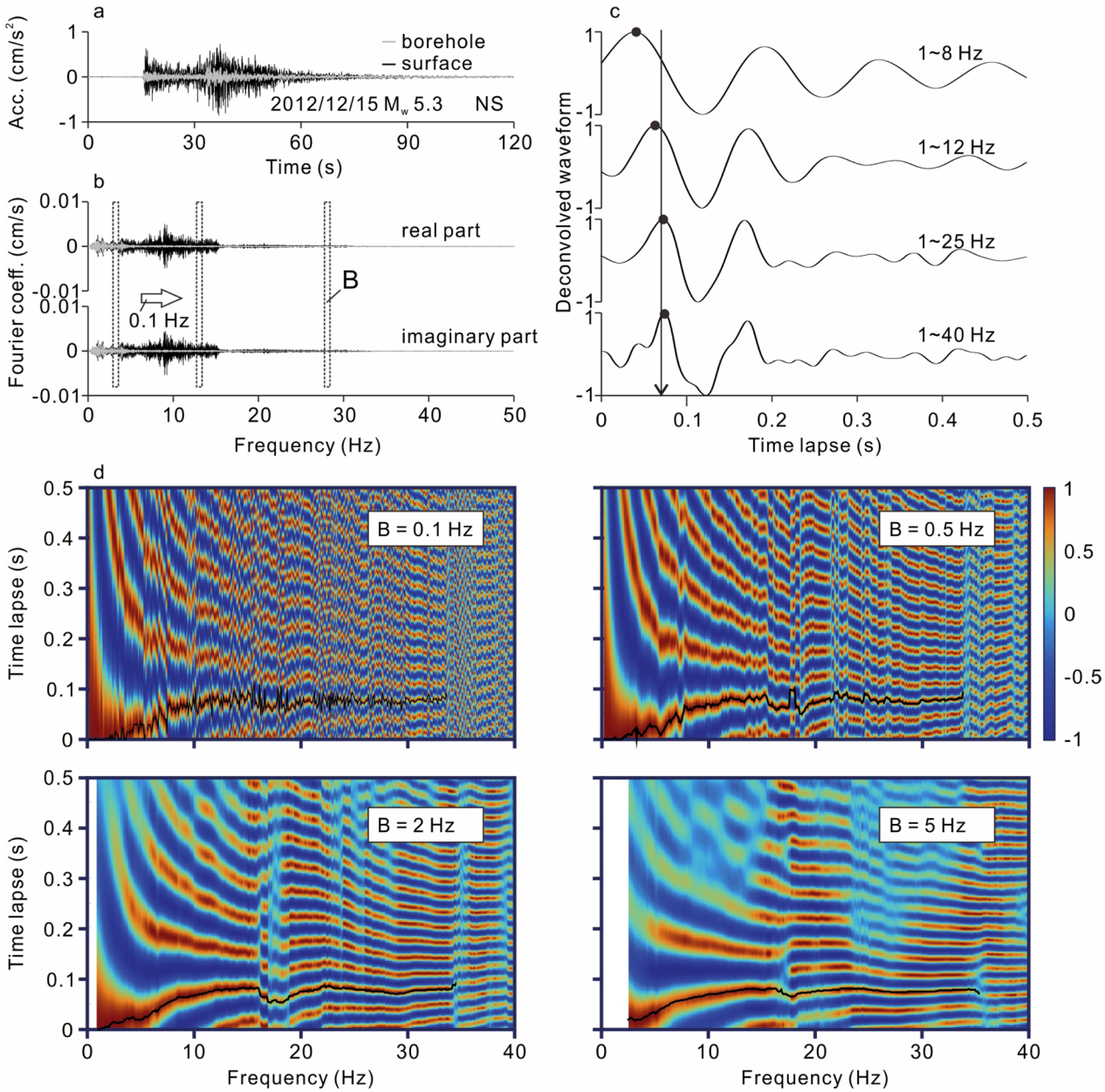

Fig. 2 Seismic interferometry with a moving-frequency window. **a** Seismic signals recorded by the station FKSH01 at 2012/12/15 in the direction of north–south. **b** The seismic signals in the frequency domain, and application method of the moving frequency window. **c** Deconvolved waveforms of different bandpass-filtered seismic signals. The black dots indicate the travel time of the shear wave traveling from the borehole to the surface, and the arrow denotes the travel time from the well-log profile. **d** Deconvolved waveforms of different moving bandpass-filtered seismic signals. The black lines indicate the travel time of the shear wave at different frequencies

the technical details of the moving-frequency-window seismic interferometry. Secondly, we calculated the frequency-varying site empirical transfer function and extracted the travel time curve with respect to frequency. Thirdly, we obtained the frequency-dependent velocity and analyzed the dispersion property of the shear wave in near-surface sediment.

Data and method

KiK-net data

KiK-net network is a strong-motion network which is operated by the National Research Institute for Earth Science and Disaster Resilience (NIED) since 1996. The KiK-net network is composed of nearly 700 seismic stations evenly deployed in Japan, and the distance between each

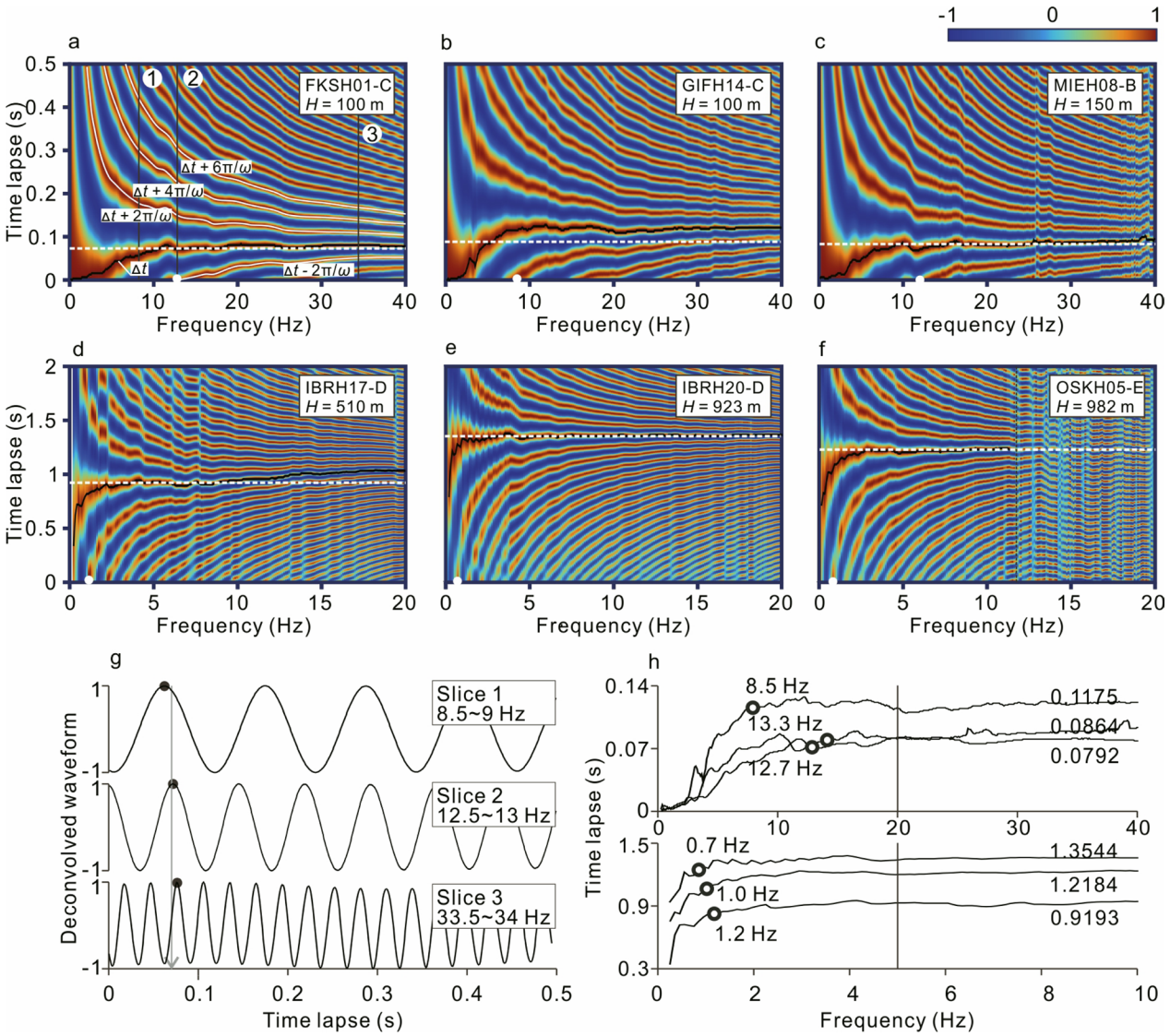

Fig. 3 **a**–**f** Deconvolution waveforms of the six stations. The black solid lines track the frequency-varying time lapse of the shear wave. The horizontal white dotted lines indicate the reference travel time from the geological profile. The letter after the station code indicates the site classification, and *H* is the borehole depth. **g** Three representative deconvolution waveforms from different filter windows, and the vertical black lines in **a** denote the position of the three slices. **h** The travel times of the six stations, and the black hollow points denote the frequency that the wavelength is equal to the borehole depth

station is about 20 km. Each station consists of a borehole and a pair of seismic sensors installed at the bottom and surface. The depths of 80% of the boreholes range within 100–200 m, and the deepest borehole is about 3500 m. A 3-D acceleration time series that lasts for 60, 120, or 300 s will be recorded when the sensors are triggered by an earthquake, and the sampling frequency is 100 or 200 Hz.

During nearly 30 years of operation, the type of the accelerometer, locations of some stations, and the algorithms for data collection and transmission have undergone some updates and iterations (Aoi et al. 2020, 2004; http://id.nii.ac.jp/1625/00001136/), which may cause the discontinuity of data. Therefore, we first selecting a continuous recording time interval for each station to eliminate the possible impact of this part. Finally, we collected 2718 seismograms recorded by 6 KiK-net stations over the course of approximately 12 years ranging from 2007 to 2019 for our research (Additional file 1: Fig. S1). As shown in Fig. 1, the 6 KiK-net stations are distributed in different areas of the Japan's Honshu Island, with different borehole depths and geological profiles (Additional file 1: Fig. S2), which ensure the universality of our

investigation. We excluded the seismic signals with the peak ground accelerations exceeding 20 cm/s^2, which ensures that the ground nonlinearly does not affect the results (Wang et al. 2019; Régnier et al. 2013; Wu et al. 2010). To eliminate the influence of the sediment anisotropy, we rotate the east–west and north–south records every 10 degrees to obtain the seismic signals in 18 directions (Additional file 1: Fig. S3). The data were calculated in the 18 directions individually and then averaged to obtain isotropic results (Sawazaki and Snieder 2013; Nakata and Snieder 2012; Miyazawa et al. 2008).

Seismic interferometry

Seismic interferometry is a technique that calculates the empirical transfer function and extracts the travel time of the seismic wave based on the wavefield information (Curtis et al. 2006). According to its calculation principles, it can be roughly divided into two categories: those based on the cross-correlation (convolution) and those based on the deconvolution (Bonilla et al. 2019; Wang et al. 2021; Nakata and Snieder 2012; Miyazawa et al. 2008). Considering that the seismic interferometry based on the deconvolution can eliminate the influence of the source and path effects, and only focuses on the site sediment (Nakata and Snieder 2012), we choose the seismic interferometry based on the deconvolution to process the seismic signals. Equation of the seismic interferometry based on deconvolution is as follows:

$$G(\omega) = \frac{S(\omega)B^*(\omega)}{B(\omega)B^*(\omega) + \varepsilon}, \tag{1}$$

where G is the transfer function, S and B represent the surface and borehole wavefield, respectively, ω is the angular frequency, asterisk is the conjugate symbol, and ε is the stability factor which is equal to 1% of the mean value of the power spectrum of the borehole seismic signals.

Application example of the method is illustrated in Fig. 2, and the steps are introduced here briefly. First, the Fourier transform is applied to the seismic signals recorded by the KiK-net station at the borehole and surface, respectively. Second, the surface wave field is divided by the borehole wave field in the frequency domain to obtain the deconvolved waveform in the frequency domain as shown in Eq. (1). Third, a 0.5-Hz-width moving bandpass filter with 0.1 Hz step length is applied to the entire waveform. Fourth, we apply the inverse Fourier transform for every filtered waveform to obtain the transfer function in the time domain. Fifth, the transfer function is interpolated 1:10,000 to improve the resolution of the result.

In general, steps and technical details of the seismic interferometry are totally the same with the previous studies (Bonilla et al. 2019; Nakata and Snieder 2012), except that we change the filter frequency band from the common 1–12 Hz to a series of 0.5 Hz width moving frequency windows with 0.1 Hz step length. The reason for selecting 0.5 Hz as the window width is as follows.

Resolution and stability are the two factors that need to be balanced when processing the seismic signals, and they are significantly affected by the choice of the width of the frequency window. Generally, as the window width increases, the resolution of the result decreases, and the stability of the result first increases and then decreases. As shown in Fig. 2c, when the filter bandwidth is too large, the stability of the result decreases, because although the effective information within the filter window increases, the noise and singular values in the window also increase. As shown in Fig. 2d, when the window

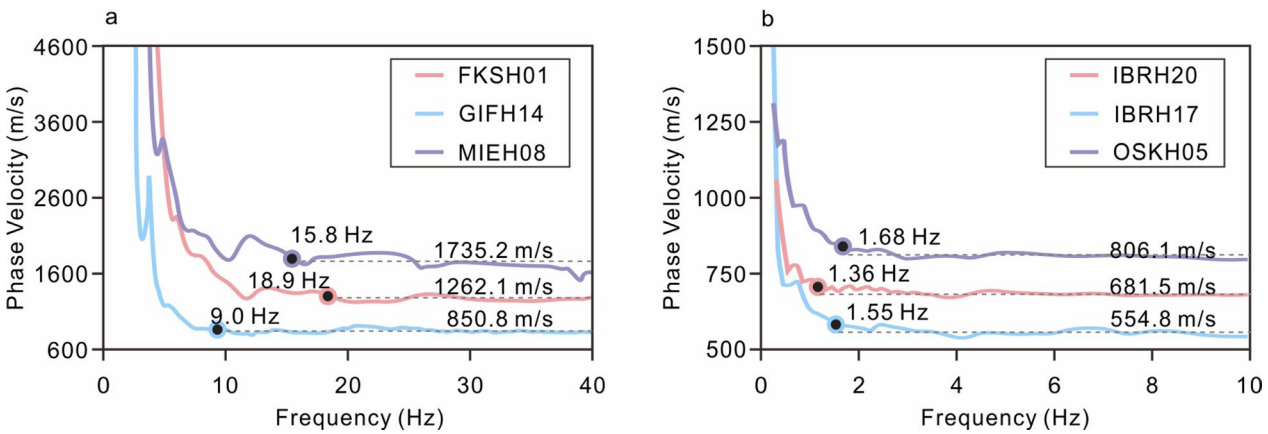

Fig. 4 Phase velocity of the shear wave at the six stations. The black dots indicate the frequency that the dispersion phenomenon disappears

width is small, the stability of the result increases as the filter bandwidth increases, because each moving window acts like a safety cabin that confines the influence of the singular values inside the window, and increased the weight of effective information. After comparison, we think that the filter bandwidth of 0.5–2 Hz is proper that can achieve the balance of the result stability and resolution. Considering the focus of our study is the frequency-dependent properties of the shear wave, higher resolution is preferred, 0.5 Hz is finally determined as the width of the moving frequency window.

Results

The transfer function of the sediments of the 6 stations is shown in Fig. 3a–f, and they have similar characteristic. We take the station FKSH01 as an example to elaborate on the results. Compared with the traditional seismic interferometry that calculates the average phase difference of the shear wave traveling form the borehole to the surface, the moving-frequency-window seismic interferometry decomposes the mixed seismic signals into a series of individual harmonic waves of different frequencies, and the phase differences of each frequency harmonic wave are calculated.

Three slices of the transfer function at three frequencies are taken and illustrated in Fig. 3g to describe the characteristics of the frequency-varying deconvolution waveform. Compared with that deconvolution waveform with the wide filter band (Fig. 2c), the deconvolution waveforms of the decomposed signals are more stable and the meaning of the peaks are clearer. As the frequency increases, the wavelength of the shear wave decreases, and the phase difference of the shear wave traveling from the borehole to the surface continuously increases. As shown in the slice 1, when the wavelength is greater than the depth of the borehole, the phase difference between the borehole and surface is less than 2π, and the peak of the time delay is the first peak. As shown in the slice 2, when the wavelength is equal to the depth of the borehole, the phase difference between the borehole and surface is equal to 2π, and the peak of the time delay becomes the second peak. Slice 3 shows the situation with shorter wavelengths and more peaks. In addition to the peaks of the time delay, other peaks indicate that the phase difference has increased or decreased by several complete cycles on top of its true value. For the traditional seismic interferometry, because the deconvolution waveform is a mixture of multiple frequencies, it is difficult to interpret the clear meaning of every peak.

According to the extracted curve of the time delay, we observed that change of the time delay over frequency can be divided into two segments: in the low-frequency range, the time delay of shear wave increases gradually with the increase of the frequency, and in the high frequency, the time delay remains constant. It should be noted that the concepts of "high frequency" and "low frequency" are not absolute, but rather determined by the relative value between the wavelength and the thickness of the sediment. We extracted the frequencies for each station that the wavelength is equal to the borehole depth, and marked them on Fig. 3h. As shown in Fig. 3h, this frequency is approximately the boundary between "high" and "low" frequencies, and the dispersion phenomenon mainly occurs when the wavelength is greater than the depth of the borehole.

In order to quantitatively study the variation of wave velocity with frequency, we averaged the time delay at high frequencies and defined it as the non-dispersive value. For stations FKSH01, GIFH14, and MIEH05, the average range is 20–40 Hz, and for stations IBRH17, IBRH20, and OSKH05, the average range is 5–10 Hz. The non-dispersive values of the travel time of the six stations are shown in Fig. 3h. At the frequencies that the wavelengths are equal to the borehole depths, the time delays are 0.0713 s, 0.1152 s, 0.0768 s, 0.8203 s, 1.1889s, and 1.0031 s for the six stations, which are 9.4%, 2.6%, 10.6%, 10.8%, 12.2%, and 17.7% less than the non-dispersive value. We also observed that for the first frequency window (0–0.5 Hz), the time delays are 0 s for the three shallow stations FKSH01, GIFH14, and MIEH08, and are 0.3371 s, 0.9437 s, and 0.7489 s for the three deep stations IBRH17, IBRH20 and OSKH05. We speculate that such differences may be caused by the resolution of the calculation method. For stations that the borehole depths are too deep, a window width of 0.5 Hz is not narrow enough to observe the information that the wave wavelength is much larger than the sediment thickness.

Divided the time delay by the borehole depth, Fig. 4 shows the calculated phase velocity of the six stations. We define the frequency corresponding to a 2% increase in comparison to the non-dispersive value as the threshold at which the dispersion phenomenon disappears. The thresholds of the six stations are 18.9 Hz, 9 Hz, 15.8 Hz, 1.55 Hz, 1.36 Hz, and 1.68 Hz for the six stations, which implies that the wavelength are about 0.67, 0.94, 0.74. 0.70, 0.54, and 0.49 times the borehole depth. In addition to the non-dispersive threshold and the one-wavelength point, we have also selected the 2 times wavelength point and 5 times wavelength point as features to illustrate the results. In general, the corresponding phase velocity is approximately 1.51 and 11.21 times the non-dispersive value (Additional file 1: Fig. S4).

Discussion

The observed changes in the phase velocity of shear wave are difficult to explain using the material dispersion theory. According to the theory and experiments related to material dispersion, the shear wave velocity only increases by less than 5% at the range of approximately a few thousand hertz, and in the seismic band, the shear wave velocity remains unchanged (Ba et al. 2016; Borgomano et al. 2017; Müller et al. 2010). However, both the trend and the magnitude of the observed change of the shear wave phase velocity differ greatly from the geomaterial material dispersion. It was observed that the phase velocity decreases rather than increases as the frequency increases, and the magnitude of the change is also several orders of magnitude greater than 5%. Considering that material dispersion theory is already quite comprehensive, other theories need to be sought to explain the observed phenomenon.

The complete earthquake process consists of three parts: the source, path, and site effects (Denolle et al. 2014; Kaklamanos et al. 2021), and our study does not involve the source and path effects of earthquake. Different source locations, source mechanisms, and magnitudes do not affect the results (Additional file 1: Fig. S5 and S6). The observed dispersion phenomenon is determined by the properties of the site sediment. Currently, the mainstream simulation of the site effect is based on the seismic ray theory, which assumes the sediment into the homogeneous layered model (Kramer 1996; Cervený 2001). However, the assumption of the "homogeneous layered" only applies to high-frequency scenarios and cannot account for the inhomogeneity of site sediment, specifically when the wavelength of the shear wave is larger than the sediment thickness.

The Newton's law, Hooke's law, and the "high-frequency assumption" are the three basic assumptions of the seismic ray theory (Cervený 2001). The "high-frequency assumption" requires that the wavelength of the shear wave is smaller than 1/3 of the scale of the change in the medium modulus, which implies that within 3 times the wavelength length scale, changes of the medium modulus can be ignored and the medium can be regarded as homogeneous. However, we noticed that the frequency band of our observation does not satisfy the "high-frequency assumption". Most of the energy of the seismic shear wave concentrates on the low-frequency band, the variation of the phase velocity mainly occurs when the wavelength is larger than the sediment thickness and variation of the modulus of the near-surface sediment cannot be neglected. The observed frequency dispersion occurs in the situations that are beyond the basic assumption of seismic ray theory.

In physics, when the wavelength of a wave is in the same order as the scale of the medium, the geometric dispersion which is determined by the boundary conditions of the modulus distribution of the medium will occur (Kolsky 1963; Shen and Yin 2016). This is another type of wave dispersion besides material dispersion, and examples include the body-wave waveguide dispersion, water wave dispersion, and seismic surface wave dispersion (Li et al. 2018; Dullin et al. 2001; Shapiro and Campillo 2004). When simulating the site effect, as a boundary condition of modeling the site sediment, the "homogeneous layered" and "inhomogeneous with modulus gradient" are not equivalent. Therefore, we speculate that the observed shear wave dispersion phenomenon is a type of the geometric dispersion caused by the inhomogeneity of the sediment (Additional file 1: Fig. S7), and whether this conjecture is reasonable requires further investigation in the future research.

Conclusions

We conduct a research about the frequency-dependent properties of the shear wave velocity in near-surface sediment based on in situ observation method. The main conclusions are as follows:

(1) Using the moving-frequency-window seismic interferometry method to process the natural seismic signals is feasible. It can improve the frequency resolution of the results, reduce the randomness and instability of the empirical transfer function, and help obtain richer and more accurate seismic wavefield information.
(2) The shear wave velocity in near-surface sediment is strongly frequency-dependent in the low frequency. When the wavelength of the shear wave is much greater than the sediment thickness, the phase velocity of the shear wave decreases sharply as the frequency increases. When the wavelength is equal to the sediment thickness, the phase velocity is approximately 10% greater than the non-dispersive value. When the wavelength is less than 0.68 times the sediment thickness, the dispersion phenomenon disappears.
(3) The observed dispersion phenomenon is beyond the scope of the material-dispersion theory and may be caused by the inhomogeneity of the sediment. It reflects the significant discrepancy between the laboratory material sample and the actual sediment structure, and revealed the frequency-dependent property of shear wave when the shear wave does not comply with the "high-frequency assumption" of the seismic ray theory.

Supplementary Information

The online version contains supplementary material available at https://doi.org/10.1186/s40623-023-01918-0.

Additional file 1. Additional details for the data, methods, and results.

Acknowledgements
We are grateful to the National Research Institute for Earth and Disaster prevention (NIED) for providing us KiK-net data. This study was financially supported by the National Natural Science Foundation of China (No. 51778260) and Natural Science Foundation of Hubei Province (No. 2022CFA014).

Author contributions
YM supported and supervised this project. HZ computed the observations and wrote the manuscript. HH, HJ, and YS discussed the results and provided comments on the manuscript.

Funding
National Natural Science Foundation of China Grant No 51778260, 2022CFA014

Availability of data and materials
Seismic data used in this study are provided by the National Research Institute for Earth Science and Disaster Resilience (Japan) and can be downloaded from website: https://www.kyoshin.bosai.go.jp/kyoshin/quick/index_en.html. Matlab code and corresponding data creating Fig. 2 are available at https://doi.org/10.5281/zenodo.6459713.

Declarations

Competing interests
The authors acknowledge there are no conflicts of interests.

Author details
[1]School of Civil and Hydraulic Engineering, Huazhong University of Science and Technology, Wuhan 430074, China. [2]National Center of Technology Innovation for Digital Construction, Wuhan 430074, China.

Received: 22 May 2023 Accepted: 5 October 2023
Published online: 26 October 2023

References

Aki K, Richards PG (1980) Quantitative Seismology: theory and methods. Freeman, San Francisco. https://doi.org/10.1017/S0016756800034439
Aoi S, Kunugi T, Fujiwara H (2004) Strong-motion seismograph network operated by NIED: K-NET and KiK-net. J Jpn Assoc Earthq Eng 4(3):65–74. https://doi.org/10.5610/jaee.4.3_65
Aoi S, Asano Y, Kunugi T, Kimura T, Uehira K, Takahashi N, Ueda H et al (2020) MOWLAS: NIED observation network for earthquake, tsunami and volcano. Earth Planet Space 72(1):1–31. https://doi.org/10.1186/s40623-020-01250-x
Ba J, Zhao J, Carcione JM, Huang X (2016) Compressional wave dispersion due to rock matrix stiffening by clay squirt flow. Geophys Res Lett 43(12):6186–6195. https://doi.org/10.1002/2016GL069312
Bonilla LF, Guéguen P, Ben-Zion Y (2019) Monitoring coseismic temporal changes of shallow material during strong ground motion with interferometry and autocorrelation. Bull Seismol Soc Am 109(1):187–198. https://doi.org/10.1785/0120180092
Borgomano JVM, Pimienta L, Fortin J, Guéguen Y (2017) Dispersion and attenuation measurements of the elastic moduli of a dual-porosity limestone. J Geophys Res Solid Earth 122(4):2690–2711. https://doi.org/10.1002/2016JB013816
Carcione JM (2007) Wave fields in real media: wave propagation in anisotropic, anelastic, porous and electromagnetic media. Elsevier
Cervený V (2001) Seismic ray theory. Cambridge University Press, Cambridge
Chabyshova E, Goloshubin G (2014) Seismic modeling of low-frequency "shadows" beneath gas reservoirs. Geophysics 79(6):D417–D423. https://doi.org/10.1190/geo2013-0379.1
Curtis A, Gerstoft P, Sato H, Snieder R, Wapenaar K (2006) Seismic interferometry—turning noise into signal. Lead Edge 25(9):1082–1092. https://doi.org/10.1190/1.2349814
Denolle MA, Dunham EM, Prieto GA, Beroza GC (2014) Strong ground motion prediction using virtual earthquakes. Science 343(6169):399–403. https://doi.org/10.1126/science.1245678
Dullin HR, Gottwald GA, Holm DD (2001) An integrable shallow water equation with linear and nonlinear dispersion. Phys Rev Lett 87(19):194501. https://doi.org/10.1103/PhysRevLett.87.194501
Field EH, Johnson PA, Beresnev IA, Zeng Y (1997) Nonlinear ground-motion amplification by sediments during the 1994 Northridge earthquake. Nature 390(6660):599–602. https://doi.org/10.1038/37586
Kaklamanos J, Bradley BA (2018) Challenges in predicting seismic site response with 1D analyses: conclusions from 114 KiK-net vertical seismometer arrays. Bull Seismol Soc Am 108(5A):2816–2838. https://doi.org/10.1785/0120180062
Kaklamanos J, Cabas A, Parolai S, Guéguen P (2021) Introduction to the special section on advances in site response estimation. Bull Seismol Soc Am 111(4):1665–1676. https://doi.org/10.1785/0120210152
Kim D, Lekic V (2019) Groundwater variations from autocorrelation and receiver functions. Geophys Res Lett 46(23):13722–13729. https://doi.org/10.1029/2019GL084719
Koedel U, Karl L (2020) Determination of the damping ratio by multi-channel spectral analysis of seismic downhole data. Soil Dyn Earthq Eng 136:106235. https://doi.org/10.1016/j.soildyn.2020.106235
Kolsky H (1963) Stress waves in solids (Vol. 1098). Courier Corporation
Kramer SL (1996) Geotechnical earthquake engineering. Pearson Education India.
Li J, Hanafy S, Schuster G (2018) Wave-equation dispersion inversion of guided P waves in a waveguide of arbitrary geometry. J Geophys Res Solid Earth 123(9):7760–7774. https://doi.org/10.1029/2018JB016127
Miyazawa M, Snieder R, Venkataraman A (2008) Application of seismic interferometry to extract P-and S-wave propagation and observation of shear-wave splitting from noise data at Cold Lake, Alberta, Canada. Geophysics 73(4):D35–D40. https://doi.org/10.1190/1.2937172
Müller TM, Gurevich B, Lebedev M (2010) Seismic wave attenuation and dispersion resulting from wave-induced flow in porous rocks-a review. Geophysics 75(5):75A147-75A164. https://doi.org/10.1190/1.3463417
Nakata N, Snieder R (2012) Estimating near-surface shear wave velocities in Japan by applying seismic interferometry to KiK-net data. J Geophys Res Solid Earth. https://doi.org/10.1029/2011JB008595
National Research Institute for Earth Science and Disaster Resilience (2019) NIED K-NET, KiK-net. https://doi.org/10.17598/nied.0004
Peng Z, Ben-Zion Y (2006) Temporal changes of shallow seismic velocity around the Karadere-Düzce branch of the north Anatolian fault and strong ground motion. Pure Appl Geophys 163:567–600. https://doi.org/10.1007/s00024-005-0034-6
Régnier J, Cadet H, Bonilla LF, Bertrand E, Semblat JF (2013) Assessing nonlinear behavior of soils in seismic site response: statistical analysis on KiK-net strong-motion data. Bull Seismol Soc Am 103(3):1750–1770. https://doi.org/10.1785/0120120240
Rydelek PA, Tuttle M (2004) Explosive craters and soil liquefaction. Nature 427(6970):115–116. https://doi.org/10.1038/427115a
Sawazaki K, Snieder R (2013) Time-lapse changes of P-and S-wave velocities and shear wave splitting in the first year after the 2011 Tohoku earthquake, Japan: shallow subsurface. Geophys J Int 193(1):238–251. https://doi.org/10.1093/gji/ggs080
Shapiro NM, Campillo M (2004) Emergence of broadband Rayleigh waves from correlations of the ambient seismic noise. Geophys Res Lett. https://doi.org/10.1029/2004GL019491
Shen Y, Yin X (2016) Analysis of geometric dispersion effect of impact-induced transient waves in composite rod using dynamic substructure method. Appl Math Model 40(3):1972–1988. https://doi.org/10.1016/j.apm.2015.09.022
Sun LF, Milkereit B, Schmitt DR (2009) Measuring velocity dispersion and attenuation in the exploration seismic frequency band. Geophysics 74(2):WA113–WA122. https://doi.org/10.1190/1.3068426

Thompson EM, Baise LG, Tanaka Y, Kayen RE (2012) A taxonomy of site response complexity. Soil Dyn Earthq Eng 41:32–43. https://doi.org/10.1016/j.soildyn.2012.04.005

Wang HY, Jiang WP, Wang SY, Miao Y (2019) In situ assessment of soil dynamic parameters for characterizing nonlinear seismic site response using KiK-net vertical array data. Bull Earthq Eng 17(5):2331–2360. https://doi.org/10.1007/s10518-018-00539-3

Wang SY, Zhuang HY, Zhang H, He HJ, Jiang WP, Yao EL, Miao Y (2021) Near-surface softening and healing in eastern Honshu associated with the 2011 magnitude-9 Tohoku-Oki Earthquake. Nat Commun 12(1):1–10. https://doi.org/10.1038/s41467-021-21418-7

Wu C, Peng Z, Ben-Zion Y (2010) Refined thresholds for non-linear ground motion and temporal changes of site response associated with medium-size earthquakes. Geophys J Int 182(3):1567–1576. https://doi.org/10.1111/j.1365-246X.2010.04704.x

Zhu C, Cotton F, Kawase H, Haendel A, Pilz M, Nakano K (2022) How well can we predict earthquake site response so far? Site-specific approaches. Earthq Spectra. https://doi.org/10.1177/87552930211060859

Publisher's Note